

# Simulation Study of Surface muon beamline, thermal muon production and extraction for the Mu 1S-2S spectroscopy experiment at D-line

Ce Zhang

March 18, 2019

## 1 Introduction

The Muonium 1S-2S spectroscopy experiment aims to measure the  $\Delta V_{1s2s}$  and the  $m_\mu/m_e$  with a higher precision at J-PARC. The experiment will use the proton beam from the 3 GeV Synchrotron ring to Material and Life Science facility (MLF), where the proton beam is injected to the graphite target to produce muons from  $\pi$ 's decay. The generated muons are extracted to one of the muon beamline, D-line. The surface muons stop in a silica aerogel target and part of them forms thermal muoniums (Mu,  $\mu^+e^-$ ). After Mu yield out of the target, the electron in the Mu's will be knocked out by lasers and thermal muons ( $\sim 25$  meV) are generated. Then these thermal muons will be extracted by electro-static lens (SOA) and then be transported into the MCP detector with the beamline, which consist of the Electrostatic deflector (ED), Electric quadrupoles (EQs) and the Bending magnet (BM). The decay positron from the incident muon or the electron produced by the field emission at the Soa lens are eliminated by the selections of the kinetic energy and the momentum using the ED and the BM in the beam line. The MCP detector is used to detect the laser ionized  $\mu^+$ .

This note describes the simulations for the D-line, the Mu production, the electrostatic extraction and the transport of the thermal muons.

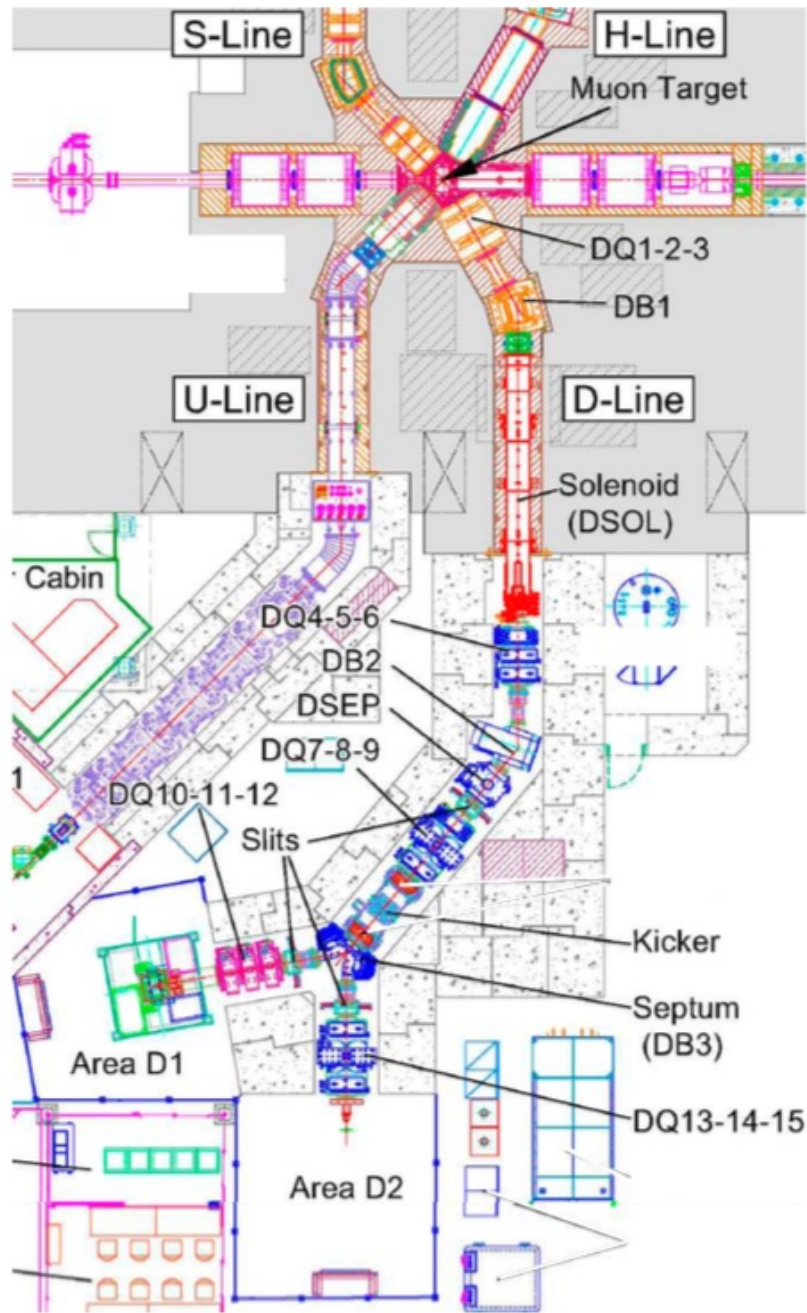


Figure 1: Schematic drawing of the Muon D-line.

## 2 Surface muon transport at D-line

D-line is the extraction line at the angle of 60 degrees backward direction of the proton beam. The surface muon will be selected during the D-line transport, which arises from the surface of the production target and have a momentum of 29.8 MeV/c (corresponds to kinetic energy 4.1 MeV).

The muon properties on the proton target was estimated by accelerator experts at MLF. The spatial distributions ( $\sigma_x = 2mm$  and  $\sigma_y = 4mm$ ) are determined based on the proton beam profiles. The momentum distributions are implemented with the range of muons in the target. Fig.2 shows the momentum dependence of the muon intensity at D-line. There is a good agreement between the simulation result and the measurement.

Figure 2 shows measured and estimated intensity as a function of muon momentum at D2 area [16]. This measurement is done with the proton beam intensity of 218 kW. The measured intensity of surface muons at 27.4 MeV/c is  $3.087 \times 10^6 \mu^+ / \text{sec}$  and the expected intensity with 500 kW proton beam is  $7.08 \times 10^6 \mu / \text{sec}$ . In comparison, totally 7063080 events at D2 area was used in the simulations.

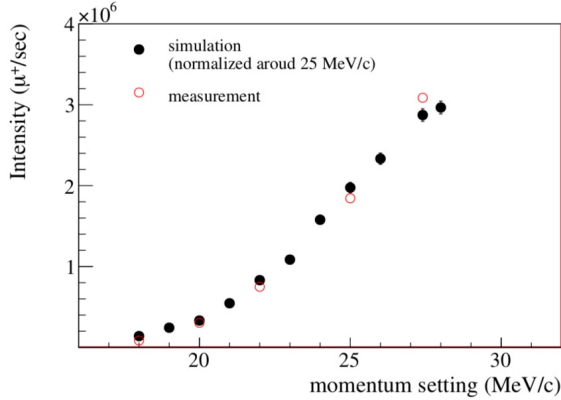


Figure 2: Momentum dependence of the surface muon intensity. Black circle and red circle show simulation and measurement, respectively. Vertical scale of the simulation is normalized by the measured value around 25 MeV/c.

To estimate the surface muon intensity and the profiles at the muonium production target, the G4beamline simulation, which is based on Geant-4 package was developed. In the simulation, the magnetic fields calculated by OPERA were implemented. The profile width in the horizontal and the vertical direction differ from each other because the beamline is not free from the momentum dispersion.

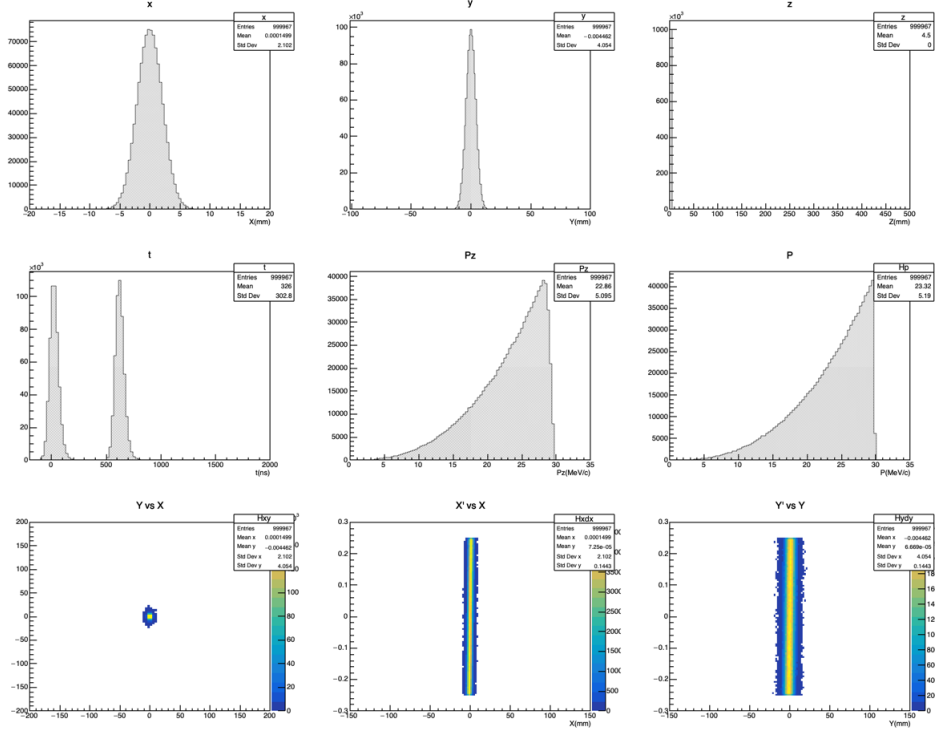


Figure 3: Initial muon beam profile before D-line transport. Both decay muon and surface muon are included.

The incident muon beam at the D2 area focused on the point 800 mm downstream from the end edge of the last triplet quadrupole (DQ15). For the better focusing of the beam, the scale factor of the last DQ triplets (DQ13-15) was optimized as shown in the Fig.4. Here only surface muon events are selected.

After the optimization, the profile of surface muon after D-line transport is shown in the Fig. 5.

### 3 Stopping distribution at the aerogel target

Geant-4 simulation was performed to obtain the fraction of the surface muon beam stopping in the target. It contains the standard physics processes such as muon creation, decay, generation of secondaries electrons, energy loss (ionization) and multiple scattering, etc. The surface muon beam distribution after D-line transport described

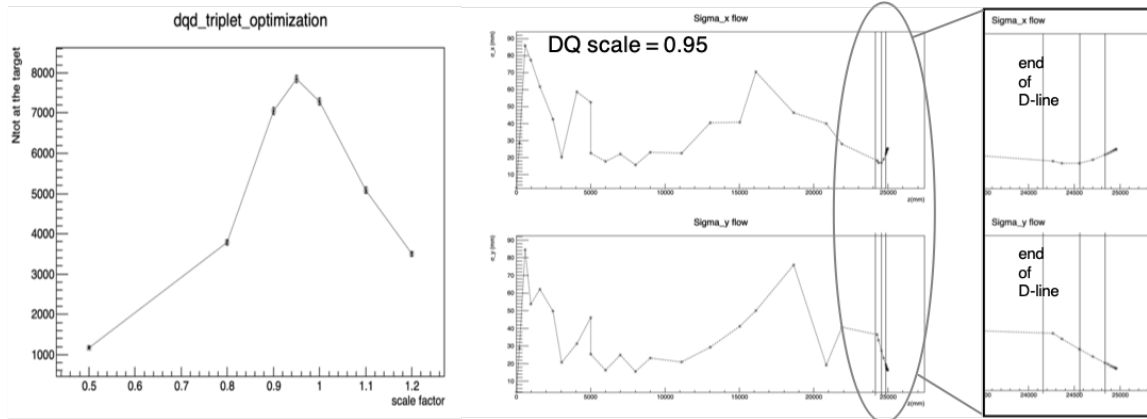


Figure 4: Initial surface muon beam profile before D-line transport

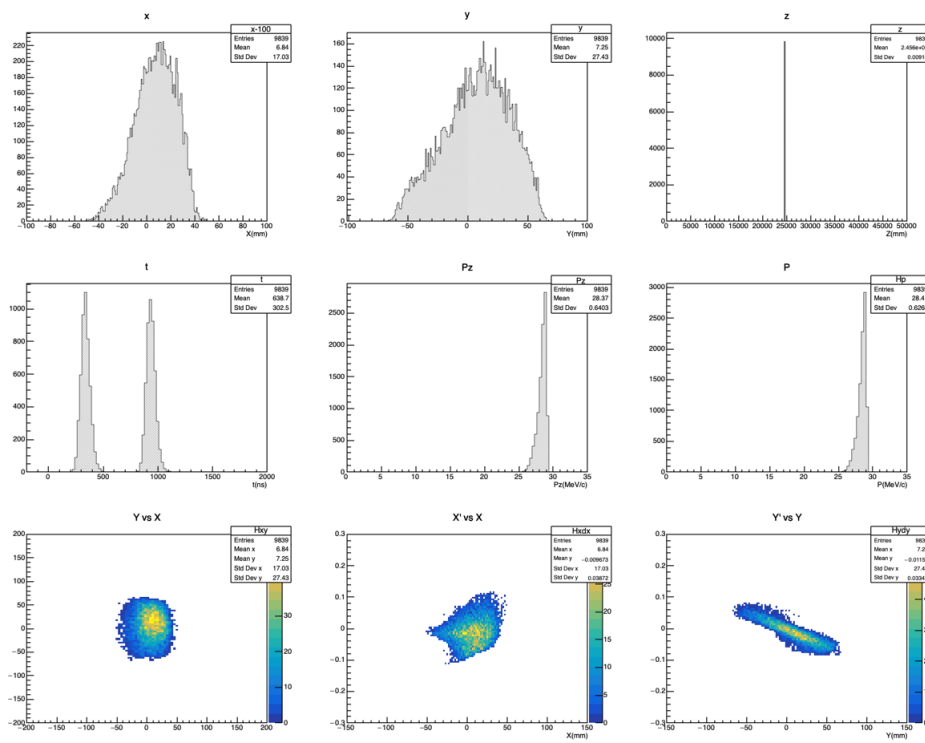


Figure 5: Surface muon beam profile after D-line transport

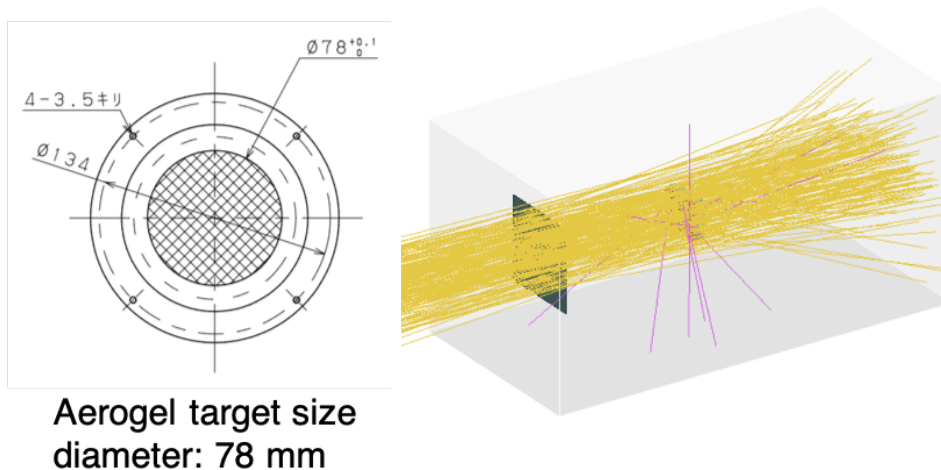


Figure 6: The size of the aerogel target and the G4 simulation scheme

in previous section were used as input.

The size of the aerogel target and the degrader were set according to the size of the chamber and the holder. The incident surface muons penetrate the SUS foil window with a thickness of 50  $\mu\text{m}$  and the diameter is 80 mm. The diameter of the degrader and the aerogel target are both 78 mm. The AL degrader was overlaid on the aerogel target. These setups take the reference from the previous  $\text{Mu}^-$  production experiment and the anti- $\text{Mu}^-$  experiment beam test on Feb. 2019.

The aerogel sample with the best  $\text{Mu}$  yield over the 23 samples from 2017 TRIUMF experiment is the aerogel target labeled S19, whose density is  $23.2 \text{ mg/cm}^3$  and the thickness is 8.8 mm. This density is different from the aerogel sample we used in the 2013 TRIUMF experiment and fitted for the diffusion model, whose density is  $30 \text{ mg/cm}^3$ . To make it consistent for the entire simulation chain, we will take the later value in the stopping simulation. The yield number will be scaled but will not vary significantly.

Based on the information above, the optimization of the Al degrader thickness was performed. This adjustment served to maximize the muon stopping density near the target surface at the downstream edge, nearest the yield and laser region.

In Fig. 8. The stopping number is maximum near 500  $\mu\text{m}$ . At most, 3270612 out of 7063080 injected surface muons stopped inside the target. The efficiency is 46.30574%. Note here, the microscopic structure of the silica aerogel is not added.

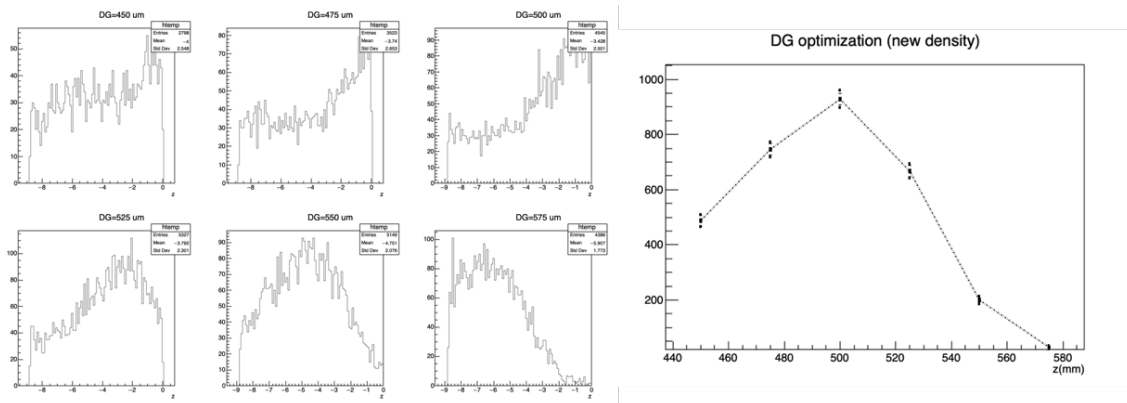


Figure 7: Optimization of the degrader thickness for the aerogel density of  $0.0322 \text{ g/cm}^3$

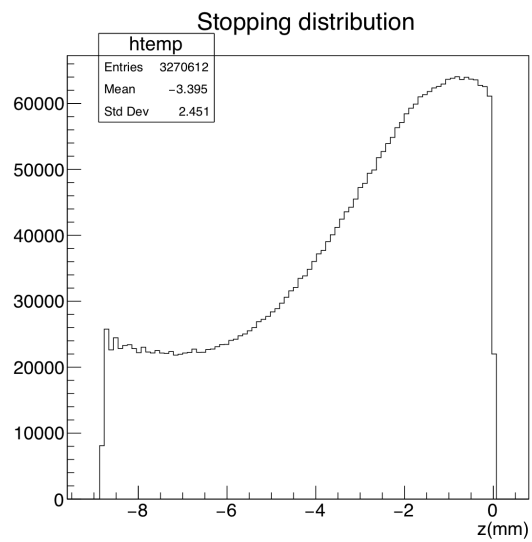


Figure 8: Stopping Distribution inside the target after the  $500 \mu\text{m}$  thickness degrader.

## 4 Diffusion simulation

The Mu production simulation was developed to estimate the Mu yield number in the laser ionization region. The diffusion model was used. The surface muon beam stopping distribution by Geant-4 described in previous section were used as input. The 52% of the stopped muon form Mu's[12]. But for the convenience of statistic, in the simulation we assume 100% of the muon events will form Mu. The 52% efficiency will be counted in the final efficiency.

The diffusion model in the target is based on a three-dimensional random walk in which each step is taken with a speed drawn from a Maxwell thermal distribution and a mean free path. The simulation parameters of the thermal temperature and the diffusion constant were determined from our measurement at TRIUMF, in which the validation of the simulation was checked and there was a good agreement between the measurement and the simulation.

The laser region is defined according to the report from Prof. Masuda Takahiko at Okayama Univ. in the Fig. 9. In the Y-Z plane, the first CW laser will ionize the Mu in the region with diameter of 0.6 mm and the second pulsed laser will shoot afterwards, whose diameter is 4 mm. There is no X-direction limit in the simulation. Mu ionized by both lasers will turn into thermal muon.

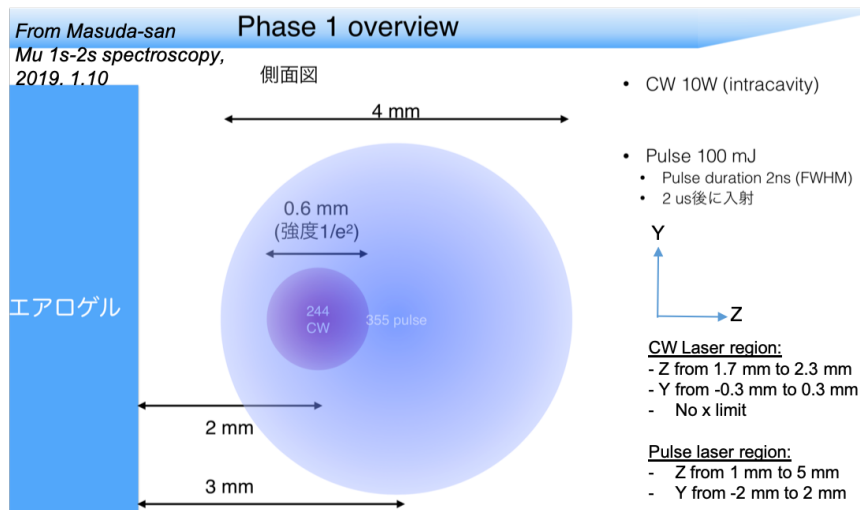


Figure 9: Laser region defined according to the report from Prof. Masuda Takahiko at Okayama Univ.



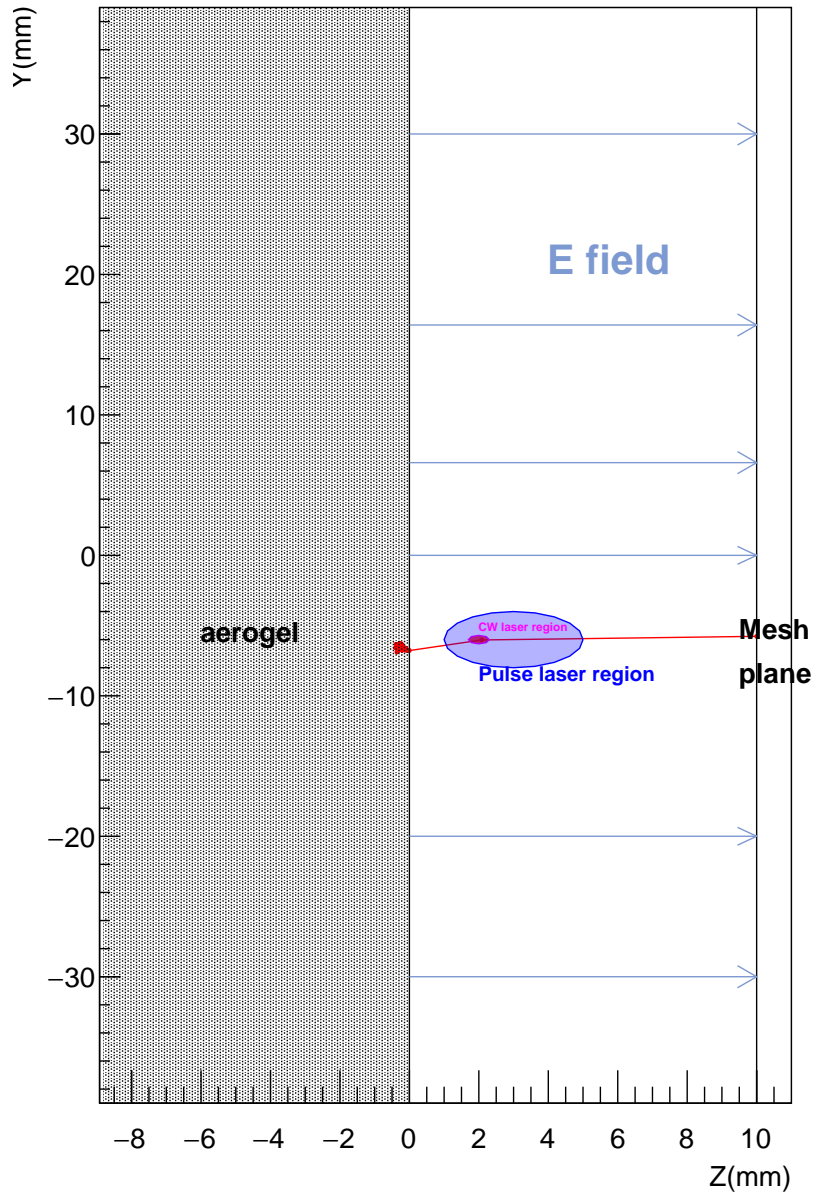


Figure 10: Schematic of the Diffusion model.

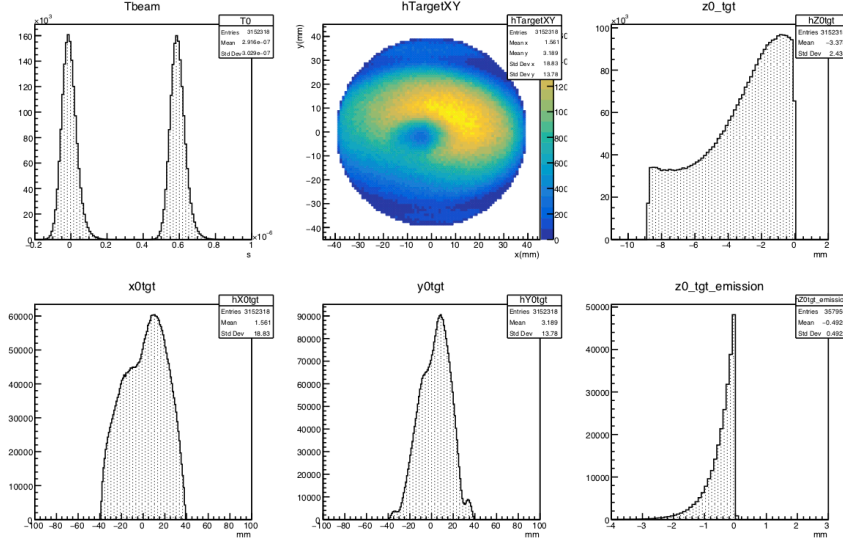


Figure 11: Initial distribution of the Mu inside the target.

Figure 12 shows the number of ionized thermal muons as a function of second laser shooting time from the time of the first surface muon beam pulse arrival. The laser pulse timing is determined to be  $1.2\mu\text{sec}$  so that the number of the thermal muons is maximized.

At last, the efficiency is calculated in this stage to be  $631/3152318 = 0.0200\%$ . Adding Mu formation efficiency 52%, it becomes 0.0104%. The laser ionization efficiency for 1S to 2S radiation and 2S to continuum radiation is unknown for now.

## 5 Thermal muon transport after laser ionization

The SOA lens are employed to initially extract the ionized thermal muons. The SOA lens consists of two mesh electrodes and three cylindrical electrodes. The first mesh electrode covers the downstream surface of the silica aerogel target.

Using the Soa electricfield and thermal muon distributions in the laser region described in previous sections, further transmission is simulated by the muSRsim package (also based on GEANT4 simulation). Figure 3.5 shows the schematic view of the beam transport simulation. The electric fields of the Soa lens, the ED, and the EQ's, and the magnetic field of the BM are generated with OPERA and implemented in musrSim. These setup come from the same setup which was used in the  $\text{Mu}^-$

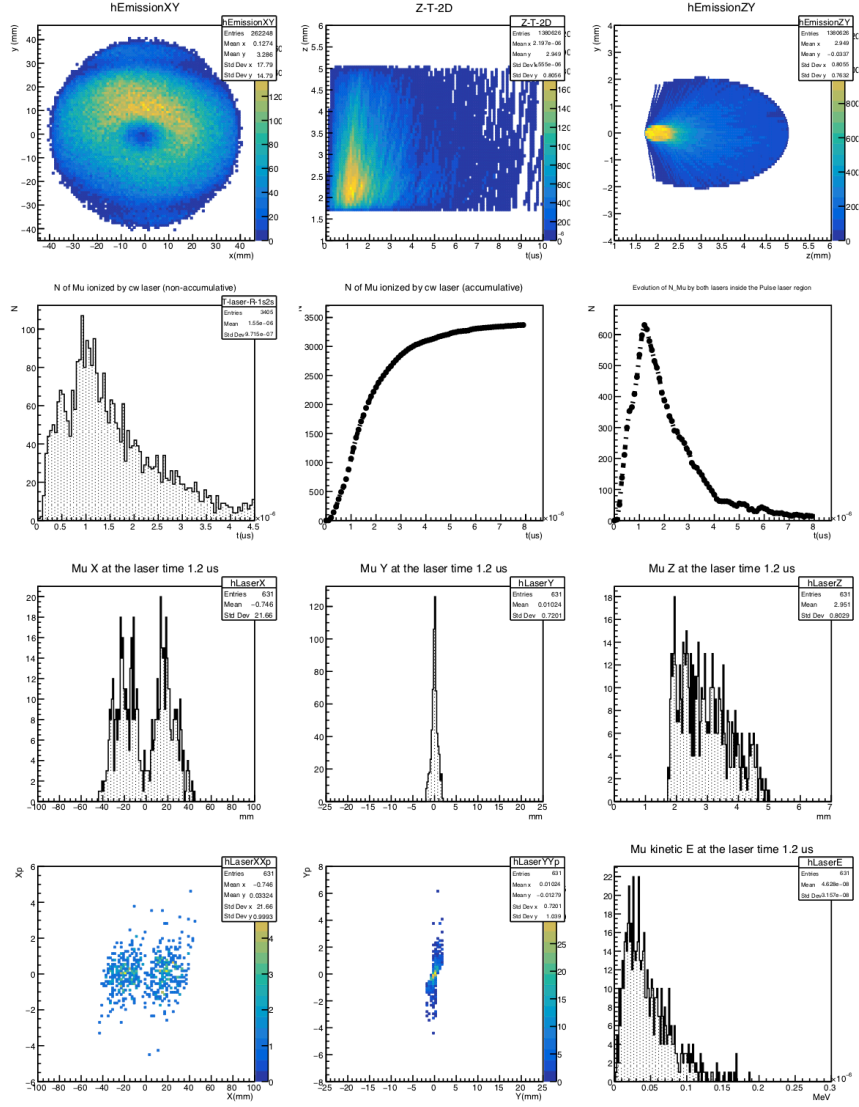


Figure 12: Evolution of Mu yield number and the time and spatial distributions

production experiment.

Figure 13 shows the schematic of the  $\text{Mu}^-$  production experiment and the typical result of the simulation of particle tracking.

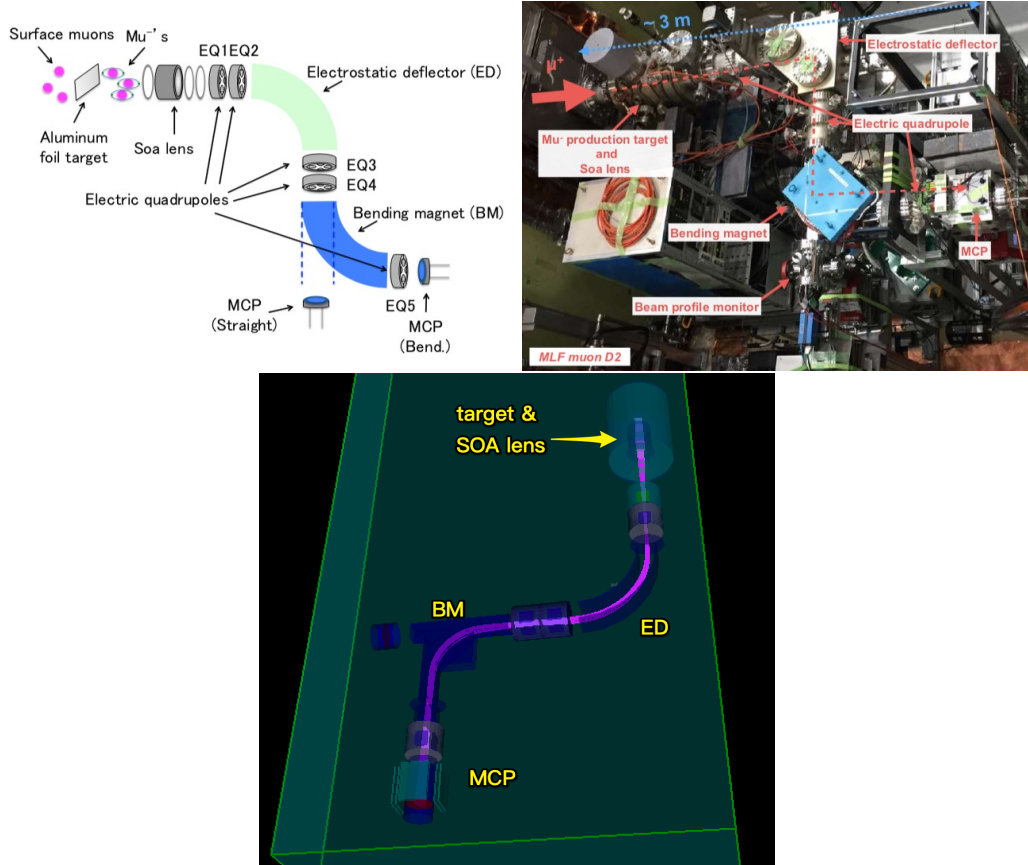


Figure 13: Schematic of the  $\text{Mu}^-$  production experiment and corresponding components and the schematic view of the beam transport simulation.

Using the distributions from previous step in the diffusion model as input, Figures 14 shows simulated phase-space distributions of the transported muon at the MCP. The number of the detected events is defined as the events within the effective area of the MCP. Table 3.2 shows the number of generated and detected events for the thermal muon in the beam transport simulation. From table 3.2, the transport efficiency of the thermal muon is  $442/631 = 70.0\%$ , including decay-loss. This efficiency would be higher if some optimizations on the beam structure focusing are performed in the future.

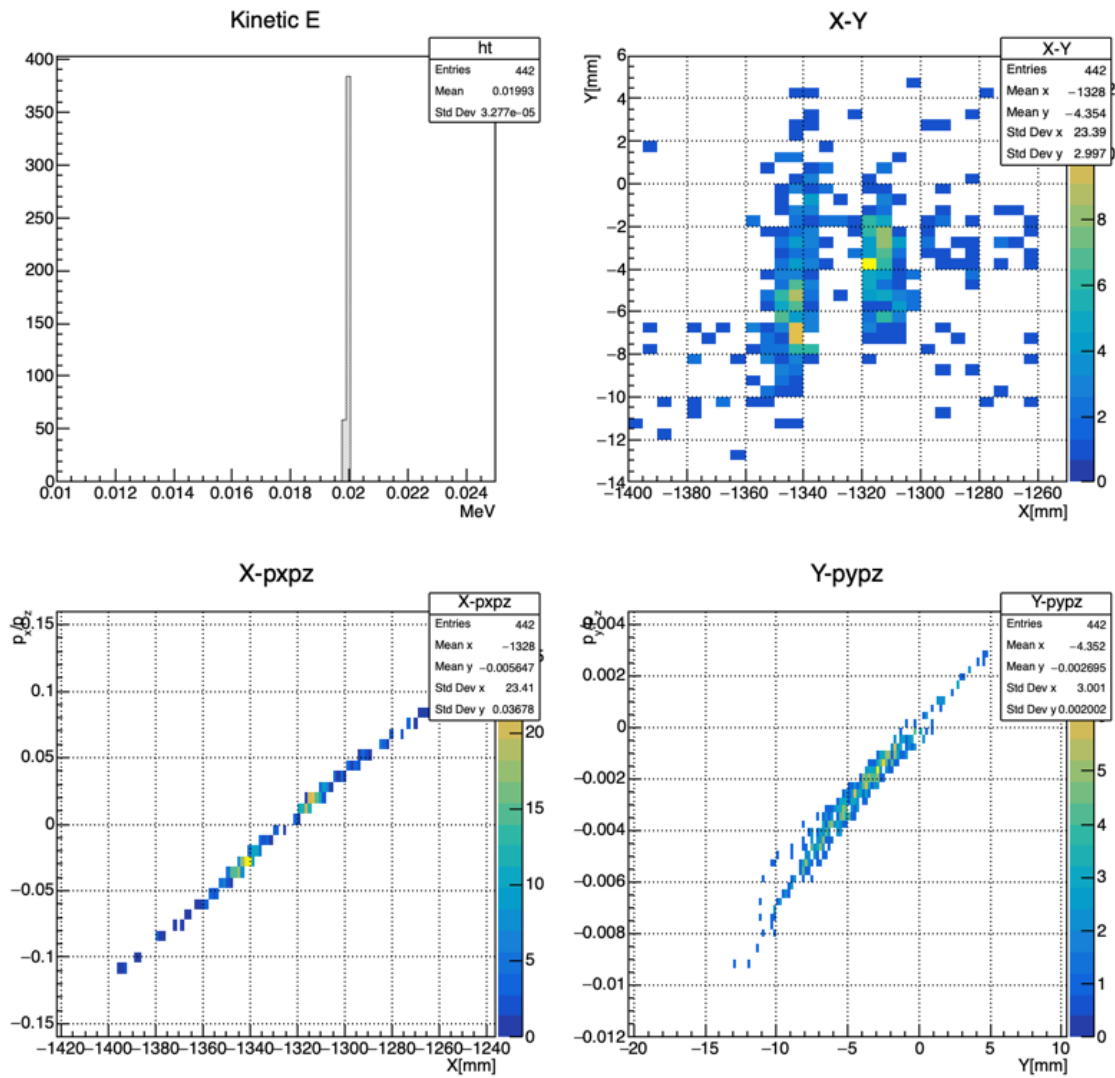


Figure 14: Simulated phase-space distributions and kinetic energy distribution for the thermal muon at the MCP

## 6 Summary

We have developed the simulation of surface muon beamline, thermal muon production and extraction for the Mu 1S-2S spectroscopy experiment at D-line. Table 1 summarizes the efficiency and the muon intensity in each step.

In total  $1.1 \times 10^8$  events was generated in the simulation at the proton target and 7063080 surface muons at the entrance of D2 area, which is comparable to the estimated actual intensity  $7.08 \times 10^6 \mu/sec$  at the D2. The efficiency of the two laser ionization is assumed to be  $\epsilon_{laser} = \epsilon_{cw} \times \epsilon_{pulse}$ . After the entire simulation chain, the muon intensity at the MCP is estimated to be  $2.39 \times 10^2 \times \epsilon_{laser} \mu^+/sec$ .

Step	Efficiency	Intensity (Hz)
$\mu^+$ at the D2 experimental area		$7.08 \times 10^6$
Surface muon stopping	46.30574%	$3.28 \times 10^6$
Mu emission	0.0104%	$3.41 \times 10^2$
Laser ionization	$\epsilon_{laser} (?)$	$3.41 \times 10^2 \times \epsilon_{laser}$
Thermal muon transmission	70.0%	$2.39 \times 10^2 \times \epsilon_{laser}$